





Formation of intermittent covalent bonds at high contact pressure limits superlow friction on epitaxial graphene

Bartosz Szczefanowicz ^{1,*}, Takuya Kuwahara ^{2,3,*}, Tobin Filleter,⁴ Andreas Klemen², Leonhard Mayrhofer,² Roland Bennewitz ¹ and Michael Moseler ^{2,5,†}

¹*INM–Leibniz-Institute for New Materials and Physics Department, Saarland University, 66123 Saarbrücken, Germany*

²*Fraunhofer Institute for Mechanics of Materials IWM, MicroTribology Center μ TC, Woehlerstrasse 11, 79108 Freiburg, Germany*

³*Department of Mechanical Engineering, Osaka Metropolitan University, 3-3-138 Sugimoto, Osaka, 558–8585, Japan*

⁴*Department of Mechanical & Industrial Engineering, University of Toronto, Toronto M5S 3G8, Canada*

⁵*Department of Physics, University of Freiburg, 79104 Freiburg, Germany*



(Received 2 November 2022; revised 13 February 2023; accepted 22 February 2023; published 30 March 2023)

Epitaxial graphene on SiC(0001) exhibits superlow friction due to its weak out-of-plane interactions. Friction-force microscopy with silicon tips shows an abrupt increase of friction by one order of magnitude above a threshold normal force. Density-functional tight-binding simulations suggest that this wearless high-friction regime involves an intermittent sp^3 rehybridization of graphene at contact pressure exceeding 10 GPa. The simultaneous formation of covalent bonds with the tip's silica surface and the underlying SiC interface layer establishes a third mechanism limiting the superlow friction on epitaxial graphene, in addition to dissipation in elastic instabilities and in wear processes.

DOI: [10.1103/PhysRevResearch.5.L012049](https://doi.org/10.1103/PhysRevResearch.5.L012049)

Introduction. Graphene is an excellent lubricant due to relevant characteristics of two-dimensional materials: strong in-plane bonds lead to high strength and wear resistance; weak out-of-plane interactions provide chemical inertness and easy shear [1]. The excellent tribological properties of graphene have been confirmed in many experiments, applying graphene as additive in liquid lubricants [2,3], as solid lubricating coating [4,5], or using it in flat-on-flat contacts, where structural lubricity leads to superlow friction [6]. Friction-force microscopy has demonstrated microscopic mechanisms of graphene lubrication such as the layer dependence of atomic stick-slip [7] and out-of-plane deformation [8]. The underlying atomic-scale mechanisms have been investigated by molecular dynamics simulations. While friction of mono- or multilayer graphene at small loads is dominated by interactions with substrates [9] and atomic-scale roughness [10], strong plastic deformation of weakly interacting metallic supports followed by graphene's rupture can cause massive friction at high loads [11].

The chemical inertness of graphene is limited by the reactivity of the carbon p_z orbital in the carbon sp^2 hybridization. Oxidation [12] and fluorination [13] of graphene deteriorate its outstanding lubrication. Here we report a steplike increase in friction on epitaxial graphene grown on SiC(0001) at normal loads which exceed a pressure of 10 GPa. We study

the friction mechanism experimentally by friction-force microscopy and theoretically by density-functional tight-binding methods. Frictional dissipation originates in the intermittent formation of covalent bonds between silicon or oxygen atoms of the sliding tip and carbon atoms of the graphene layer, which are stabilized by a rehybridization of the carbon atoms into an sp^3 configuration. The threshold pressure of the high-friction regime is reached even at moderate loading force in the center of nanoscale asperities, which are plastically flattened at the same pressure, leading to a limitation of friction forces for increasing normal pressure.

Experiment methods. The graphene/SiC(0001) sample was prepared by the research group of Thomas Seyller (University of Technology Chemnitz) by the thermal decomposition method [14]. An average coverage of 0.9 monolayers (ML) was confirmed by photoelectron spectroscopy. Atomically flat terraces of the substrate were covered with monolayer graphene. Small patches of double-layer graphene were limited to the vicinity of step edges as confirmed by Kelvin probe force microscopy and an analysis of measured step heights [15]. Small patches of bare surface area were identified by a drastically increased friction. In the ultrahigh-vacuum chamber, the samples were degassed for several hours at a temperature of 600 °C.

For atomic force microscopy (AFM) experiments, the cantilevers (PPP-ContR silicon cantilevers, NANOSENSORSTM) were introduced to the ultrahigh-vacuum system and degassed for a few hours at a temperature of 120 °C. Normal and lateral spring constants of individual cantilevers were calibrated using the geometrical beam-calibration method [16]. The tip radius of 5–10 nm was estimated after the experiments from transmission electron microscopy (TEM) images (JEOL JEM 2100 TEM).

*These authors contributed equally to this work.

†michael.moseler@iwm.fraunhofer.de

Published by the American Physical Society under the terms of the [Creative Commons Attribution 4.0 International](https://creativecommons.org/licenses/by/4.0/) license. Further distribution of this work must maintain attribution to the author(s) and the published article's title, journal citation, and DOI.

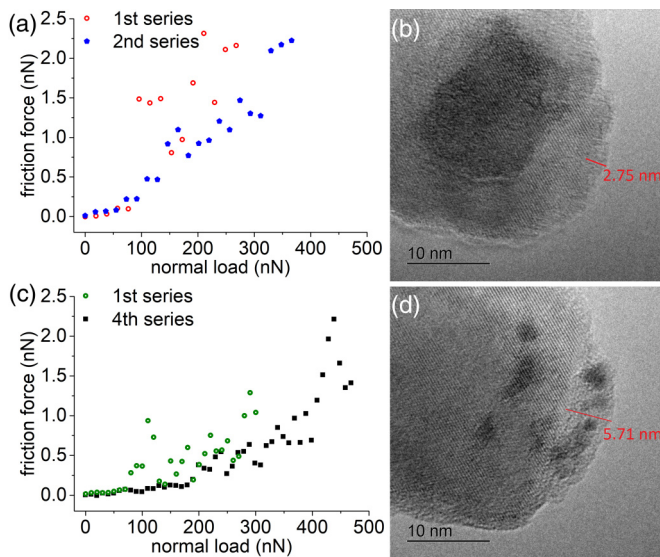


FIG. 1. Friction force as function of increasing applied normal load recorded between an oxidized silicon tip and epitaxial graphene grown on a SiC(0001) substrate. Results in (a) and (c) were recorded with the tips subsequently imaged by transmission electron microscopy in (b) and (d). Atomic planes of the single-crystal structure of the silicon tips appear as lines, the surface oxide at the top apex as amorphous layers.

Friction was measured using an Omicron VT AFM XA in ultrahigh vacuum at 1×10^{-10} mbar and room temperature. Experiments were conducted on areas covered by monolayer graphene, which were previously located by noncontact-mode AFM [15]. Each experiment consisted of a few series of scans with increasing normal load by a constant step of either 10 nN [Fig. 1(c)] or 18 nN [Fig. 1(a)]. The scan size was of $8 \times 2 \text{ nm}^2$ with a scan speed of 60 nm/s for data shown in Fig. 1. The frictional behavior reported in Fig. 1 is not influenced by changing the scan speed between 10 and 100 nm/s. The displacement of the tip position upon changing the normal load due to the cantilever tilt was compensated [17]. Friction was calculated as the average lateral force for forward and backward scans.

Experiment observations. Friction was recorded as the lateral force acting on the tip of an atomic force microscope when the tip was sliding over the graphene at varying normal forces. The experiment procedures for the AFM experiments have been described in Ref. [18]. In summary, the graphene/SiC(0001) samples were grown by the thermal decomposition method [14] and cleaned before experiments by annealing in ultrahigh vacuum (UHV). Lateral forces were recorded in UHV by scanning the AFM tip in contact over atomically flat areas of monolayer graphene and measuring the lateral-force induced torsion of the AFM cantilever. Friction was quantified as the average of lateral forces for scanning areas which were large as compared to the superstructure of the SiC(0001) surface. For smallest tip radii of a few nanometers, we used standard silicon tips sharpened by oxidation (Nanosensors PPP).

Typical results for friction versus normal load are presented in Fig. 1 together with TEM images of the tips recorded

after the friction experiments. For the first contact of an oxidation-sharpened silicon tip [Fig. 1(a)], friction is very low with a linear load dependence and a corresponding friction coefficient of 0.0016 for normal forces up to 80 nN. For a load of 100 nN, friction suddenly increases by one order of magnitude. For higher normal loads the friction values tend to even higher values, however with significant scatter in the data. With increasing normal load, friction sometimes even drops like in the data recorded at 160-nN load compared to the data recorded at 140 nN.

When we repeat the experiment with the same tip starting again at low normal load, we find the same linear low-friction regime and the transition to the high-friction regime. The transition to the high-friction regime is more gradual than in the first run. High-friction values above 2 nN are reached only at a load above 340 nN, compared to 200 nN in the first run. After these two experiments, the tip was removed from the vacuum system and immediately imaged by TEM. The image in Fig. 2(b) confirms the crystalline structure of the silicon tip and an amorphous silicon oxide surface layer on the tip apex of about 2.75-nm thickness. The overall radius of the oxidized apex can be estimated to be 5–10 nm.

Results for a different AFM tip are shown in Figs. 1(c) and 1(d). The linear low-friction regime with a coefficient of 0.0075 extends to a normal load of 80 nN in the first series of friction measurements, followed by a steplike increase in friction. Again, the high-friction values generally increase with increasing load but exhibit significant scatter. At a load of 140 nN, friction even returns to a value as low as expected for the linear low-friction regime. After repeating the load-variation experiment three times with this tip, the transition to the high-friction regime in the fourth run occurs at a load of 200 nN and values above 2 nN are reached at a load of 430 nN. The TEM image recorded after this fourth run reveals an apex oxide layer of 5.7-nm thickness and an estimated radius of 5–10 nm. Entering the high-friction regime does not damage the graphene or the underlying substrate, as we have confirmed by topographic imaging of the area before and after the friction experiments. One high-resolution example is provided in Fig. S1 in the Supplemental Material (SM) [19].

The experiments demonstrate a high-friction regime above a threshold load, which leaves the graphene layer intact. This regime is characterized by a superlinear increase in friction as function of load and irregular jumps between friction levels. Threshold load and friction increase are shifted to higher normal forces in repeated experiments with the same tip, suggesting that the sharpness of the tip and thus the effective contact pressure is reduced in experiments at high load. We have performed atomistic simulations to reveal the friction and deformation mechanisms underlying these observations.

Simulation methods. Atomistic details on the friction dynamics between a graphene/SiC(0001) and Si tip were investigated using the self-consistent charge-density functional tight-binding molecular dynamics (MD) method [20] as implemented in the ATOMISTICA software suite [21]. Since the topmost surface of the Si tip is covered with an amorphous SiO_2 ($a\text{-SiO}_2$) layer (Fig. 1), we modeled a contact between a graphene/SiC(0001) and an $a\text{-SiO}_2$ surface. The graphene/SiC(0001) surface was constructed from a monolayer graphene, a carbon interface layer, and a C-face

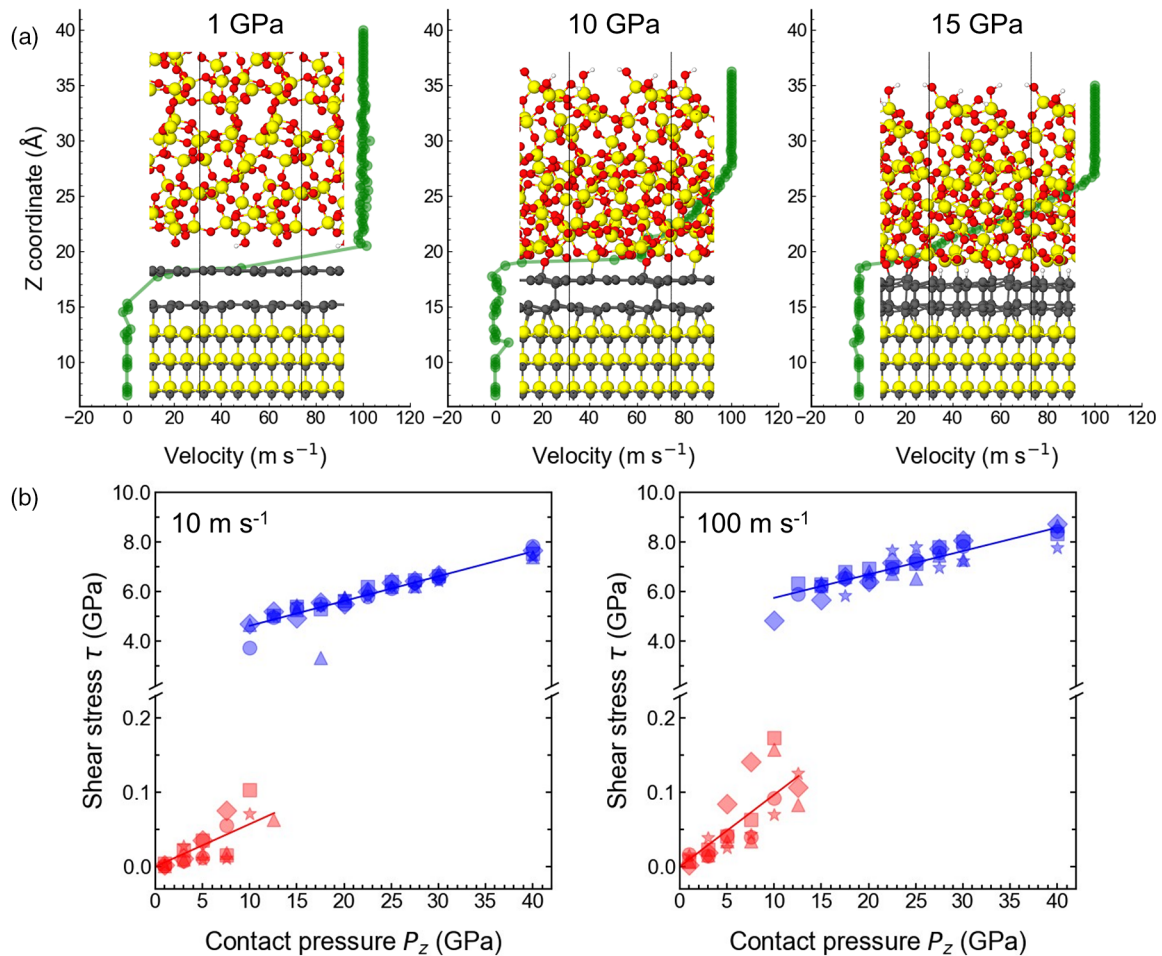


FIG. 2. (a) Simulation setup of silicon carbide with graphitic interface layer, graphene, and one of five amorphous silicon oxide configurations. Colors signify silicon (yellow), oxygen (red), carbon (gray), and hydrogen (white); sticks between balls indicate a chemical bond. Snapshots are taken from the middle of the 0.3-ns simulation period for a contact pressure of 1, 10, and 15 GPa (temperature $T = 300$ K and sliding velocity $v = 100$ m/s). Green data points report the sliding velocity as function of the normal coordinate and indicate the location of the shear plane. (b) Simulated shear stress vs contact pressure for five different silicon oxide configurations which are represented by different symbols. Red symbols indicate absence of chemical bonds between graphene and silicon oxide atoms; blues symbols indicate the formation of at least one such chemical bond between a carbon atom and a silicon or oxygen atom (temperature $T = 300$ K). Shear stress is calculated for the last 10% of 3-ns simulated sliding time at 10 m/s and of 0.3-ns sliding time at 100 m/s.

SiC(0001) surface with six layers in a periodic cell with dimensions of $9.2 \times 10.7 \times 50.0 \text{ \AA}^3$. The α -SiO₂ samples, containing 50 Si and 100 O atoms, with the same xy dimensions and a density of 2.2 g cm^{-3} were prepared by quenching SiO₂ melts under periodic boundary conditions along the three Cartesian directions while keeping the cell size constant. A slab geometry was created by cutting the α -SiO₂ bulk perpendicular to the z axis and introducing a vacuum layer. Undercoordinated Si and O atoms on both surfaces were terminated with OH groups and H atoms, respectively.

Sliding MD simulations were performed for 0.3 ns with the Pastewka-Moser-Moseler pressure-coupling algorithm [22]. Top and bottom layers of the SiO₂ and graphene-SiC slab were kept rigid, respectively. A normal pressure P_z ($1 \leq P_z \leq 40$ GPa) and sliding speed v of 100 ms^{-1} were imposed on the rigid layer of α -SiO₂ along the x axis, whereas the positions of the rigid layers of the graphene-SiC(0001)

surface remained unchanged. The sliding speed of 100 m/s is 10 orders of magnitude larger than that in the experiments. The use of such high a sliding speed is essential to simulate a long sliding distance and sufficiently sample phase space, and typical in atomistic simulations. In principle, the sliding speed has to be much smaller than the speed of sound in solids so that the heat generated at the sliding interface can be dissipated to surrounding bodies (which is modeled by coupling the thermostat to the system in this study). Considering that the speeds of sound in SiC (~ 11 km/s) and silica (~ 6 km/s) are much higher than the sliding speed of 100 m/s in the simulations, we think that this value allows us to properly model interfacial dynamics of graphene with SiC and SiO₂ under shear.

The system temperature T was kept constant at 300, 500, and 1000 K using a Langevin thermostat [23] acting only along the perpendicular to the sliding direction. The equations of motion were integrated with a time step of 0.5 fs using

the velocity Verlet algorithm [23]. The shear stress τ was calculated from the forces along the x axis acting on the rigid layers of SiO_2 and averaged over the last 0.1 ns. To investigate the effect of the sliding speed, another set of simulations with a lower sliding speed of 10 ms^{-1} was performed at $T = 300 \text{ K}$ for 3 ns (corresponding to the sliding distance of 30 nm) while keeping the other parameters unchanged. The shear stress is calculated by summing the force component along the sliding direction on all atoms in the top rigid layer and then dividing by the lateral area of the simulation cell.

Simulation results. The sliding contact between silicon oxide and an epitaxial graphene layer on $\text{SiC}(0001)$ was modeled in a quantum-mechanical molecular dynamics simulation based on a self-consistent charge density-functional tight-binding (DFTB) method [20]. The simulation allows us to describe pressure- and shear-induced plastic events and resulting structural changes at the tribological interface. The two surfaces were approached to a preset normal pressure and the shear stress across the interface was evaluated during sliding. The simulation setup and a summary of results are provided in Fig. 2. To account for variability in the amorphous structure of the silicon oxide, five different structural configurations were implemented for comparison and averaging. Surface dangling bonds on silicon and oxygen atoms were passivated by adding hydroxyl groups and hydrogen atoms, respectively. We have tested the reliability of DFTB by simulating selected trajectories with first-principles density-functional theory. The results are the same in terms of transition pressure and numbers for shear stress (see Fig. S3 in SM).

Figure 2(a) presents snapshots for one configuration sliding at contact pressures of 1, 10, and 15 GPa. With increasing pressure, the silicon oxide and the graphene– $\text{SiC}(0001)$ are compressed. Chemical bonds form between carbon atoms of the graphene layer and the underlying carbon interface layer on the $\text{SiC}(0001)$ surface, but also between carbon atoms of the graphene layer and oxygen or silicon atoms of the oxide surface. Analysis of the bond formation reveals a preferred local tetragonal sp^3 hybridization, i.e., that nearest-neighbor carbons in the graphene layer bind to the carbon interface layer below and to silicon or oxygen above, respectively. Singular C–Si bonds without corresponding C–C bonds of nearest neighbors are observed only for undercoordinated, reactive Si atoms at the oxide surface (see Fig. S4 in SM).

Figure 2(a) also shows the velocity profile of atoms across the simulation cell and thus indicates the shear plane. For a pressure of 1 GPa, the graphene layer slides on the supporting SiC with roughly 20% of the silicon oxide velocity. When C–C bonds between graphene and SiC have formed at 10-GPa pressure, the graphene completely rests with the SiC substrate and the shear plane is entirely between graphene and silicon oxide. At a pressure of 15 GPa, the shear is accommodated by deformation of the silicon oxide into a depth of 1 nm.

Values for the shear stress are summarized in Fig. 2(b) for simulations of all five silicon oxide configurations and for two different sliding velocities. For contact pressures up to 10 GPa, we observe a very low shear stress with an average coefficient of shear stress divided by normal stress of 0.01. We observe a steplike increase in shear stress by a factor of 50 at a critical contact pressure between 10 and 13 GPa. All silicon oxide configurations are in the high-friction state for

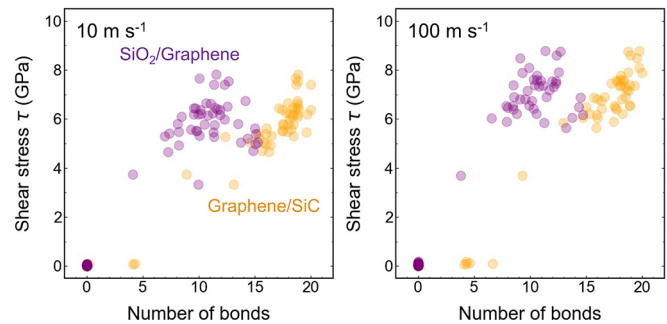


FIG. 3. Shear stress as function of the number of chemical bonds. Yellow symbols represent C–C bonds between graphene and SiC , purple symbols C–O and C–Si bonds between graphene and silicon oxide. Data represent simulation results for five different silicon oxide configurations at a sliding velocity of 10 (left) and 100 m/s (right) (temperature 300 K, contact pressures between 1 and 40 GPa as indicated in Fig. 2(b)). Note that the formation of C–C bonds alone does not necessarily lead to high shear stress.

contact pressure of 15 GPa and higher. The transition occurs at 10.1 GPa for the lower simulated sliding speed of 10 m/s, compared to 12.7 GPa the higher sliding speed of 100 m/s (see Fig. S6 in SM). We have also performed simulations at the sliding speed of 100 m/s for higher temperatures and found that the transition pressure shifts from 12.7 to 10 GPa at higher temperature (see Figs. S7 and S8 in SM). Overall, the simulation results let us expect a transition pressure of about 10 GPa for lower velocities. Please note that the system may show fluctuations between the low-friction and the high-friction state at the transition. In Fig. 2(b) we find for both sliding velocities one silicon oxide configuration in the low-friction state at a contact pressure of 12.5 GPa after having exhibited high friction at 10 GPa.

The steplike increase in shear stress is directly related to the formation of chemical bonds between the graphene layer and oxygen or silicon atoms of the silicon oxide, as analyzed in Fig. 3. The shear stress increases with the number of chemical bonds between graphene and silicon oxide. Please note that the shear stress remains close to zero when the first bonds between graphene and SiC are observed, while it increases significantly as soon as bonds between graphene and silicon oxide are formed. A strong correlation between shear stress and the number of bonds across the graphene–silicon oxide interface is also found in their respective fluctuations within simulated trajectories, while there is no correlation between the fluctuations in the number of graphene– SiC bonds and the shear stress. One example for this correlation is provided in the Supplemental Material [19] (Fig. S10 in SM).

The compression of the system under increasing pressure reduces the distance between graphene and SiC and between graphene and silicon oxide and thus is the origin of bond formation. Starting from a pressure of 7.5 GPa, we also observe an increase of bonds within the silicon oxide and, consequently, an increase in the number of overcoordinated silicon and oxygen atoms. For the contacting surface, the plastic events in the silicon oxide result in a densification and in an overcoordination of silicon and oxygen atoms, but not in the formation of reactive species at the surface. With

increasing pressure, transfer of passivating hydrogen or of oxygen to the graphene or along the surface can open bonds for reaction with the graphene. At contact pressures above 12.5 GPa, the formation of a high density of chemical bonds with graphene leads to a shift of the shear plane into the silicon oxide, when the amorphous structure becomes the weakest part of the system.

Discussion. Experimental results and tight-binding simulations reveal that the outstanding lubrication by epitaxial graphene is limited by a threshold load, above which the formation and rupture of covalent out-of-plane bonds between graphene and the sliding oxide tip causes strong friction. We will relate experimental observations to simulation findings to reveal the mechanisms underlying the transition to the high-friction regime.

The most prominent observation is a steplike increase of friction force by a factor of 10 in AFM experiments and of shear stress by a factor of 50 in simulations. The threshold normal force in AFM experiments for entering the high-friction regime is about $F_N = 100$ nN. The corresponding maximum contact pressure in the Hertz model can be estimated as

$$p_0 = \frac{1}{\pi} \left(\frac{6F_N E^*}{R^2} \right)^{1/3} \quad \text{with} \quad \frac{1}{E^*} = \frac{1 - \nu_{6H-SiC}^2}{E_{6H-SiC}} + \frac{1 - \nu_{SiO_2}^2}{E_{SiO_2}}. \quad (1)$$

With $E_{SiO_2} = 75$ GPa, $E_{6H-SiC} = 400$ GPa [24], $\nu_{SiO_2} = 0.18$, $\nu_{SiC} = 0.16$, and thus $E^* = 65.2$ GPa, the threshold contact pressure is $p_0 = 14.9$ GPa for a tip radius of $R = 5$ nm and is $p_0 = 9.4$ GPa for a tip radius of $R = 10$ nm. With these tip radii, estimated from the TEM images in Fig. 1, the range of transition pressures includes the threshold predicted by the simulations of $p = 10$ GPa.

On atomic scale, the contact pressure is expected to exhibit large fluctuations for an amorphous tip pressing against a flat surface [25]. The transition may thus occur even at lower normal forces than expected for a given tip radius. On the other hand, a contact pressure of 12.5 GPa reaches the expected yield strength of silicon oxide, even in nanometer-scale structures [26,27]. The increase in transition force in repeated experiments indicates that sharp asperities at the tip apex, which produce the pressure necessary for bonding, are flattened by plastic deformation. This picture is supported by the simulations, which register plastic events and a densification of silicon oxide for pressures exceeding 7.5 GPa. Covalent-bond formation at sharp asperities and plastic deformation of these asperities contribute to the irregularity in the evolution of the high-friction regime in simulations and in the experiments. Details of the evolution in the transition regime depend critically on the atomic configuration of the amorphous tip, as reflected in experiments with different tips and in the simulations for different silicon oxide configurations. Only when the contact pressure exceeds 15 GPa, the simulated shear stress becomes comparable for all silicon oxide configurations. In this high-pressure regime, the shear plane shifts from the graphene–silicon oxide interface into the silicon oxide. We suggest that this regime is not accessible in AFM experiments due to expected plastic yield of the sharp tip.

The simulations reveal the atomistic mechanics underlying the high-friction regime. Friction is caused by the formation of out-of-plane bonds between the graphene on the surface and silicon or oxygen atoms of the tip, the buildup of elastic energy when stretching the bonds and deforming their environment, and the fast release of the energy when the bonds rupture. The formation of these friction-related bonds is supported by additional mechanisms which are activated by the increasing contact pressure. Elastic and plastic deformation of the silicon oxide leads to a densification at the interface and thus to an increase in available binding partners. High contact pressure also initiates out-of-plane bonds between carbon atoms in the graphene layer and the carbon termination of the SiC(0001) substrate. Carbon–oxygen and carbon–silicon bonds form next to these carbon–carbon bonds and thus establish a local sp^3 configuration. The rehybridization of bilayer graphene under compression and its implications have previously been studied by simulation and in experiments. Barboza *et al.* predicted the formation of a hydroxylated diamond layer under compression and complemented this simulation results with experiments indicating the inhibition of electrical charge injection into the diamondlike materials [28]. Gao *et al.* reported a diamondlike hardness and reduced electrical conductivity for bilayer graphene on SiC(0001) under pressure, with corresponding findings in density-functional theory calculations [24]. An atomic-scale manifestation of pressure-induced hybridization in graphene–SiC(0001) was detected by high-resolution force microscopy with a single-molecule tip [29]. These reports and our own results describe a mutual stabilization of C–C bonds between the graphene layers and bonds out of the bilayer involving nearest neighbors of C–C bonded carbon. It is however important to note that neither the densification of the silicon oxide nor the formation of carbon–carbon bonds alone leads to increased friction. The high-friction regime is directly related to the formation of carbon–silicon and carbon–oxygen bonds.

A quantitative comparison of simulated shear stress and measured friction force requires a contact mechanics and a friction model. The simplest approach is to integrate the simulated shear stress over the contact area using the contact-pressure distribution predicted by the Hertz model. The calculated friction force is by a factor of 3–4 higher than measured in the low-friction regime and by orders of magnitude higher in the high friction regime, reaching values of $F_F = 50$ nN for normal forces of $F_N = 200$ nN (see Fig. S11 in SM). Such discrepancies can be expected because of three differences between experiment and simulation (see SM for detailed discussion). First, the sliding velocity is orders of magnitude lower in the experiment, impeding direct comparison of molecular dynamics and friction-force microscopy [30]. Second, our AFM tips experience flattening due to plastic deformation lowering the contact pressure and thus friction. Third, the predicted shear stress in the high-friction regime depends critically on the yield stress of the tip-apex material, which decreases with decreasing silica density and increasing hydrogen contents [31], parameters which are not known for the microfabricated AFM tip.

Limits of superlow friction, often classified as superlubricity, have been described before. In the framework of the Prandtl-Tomlinson model, elastic instabilities lead to fric-

tion on two-dimensional sheets where local deformations have to be considered [32]. In macroscale contacts, the high pressure under asperities leads to wear of graphene and concurrent increase in friction [33,34]. In technological application, contacting surfaces have a finite roughness and the contact pressure at the apex of roughness asperities can be orders of magnitude higher than the nominal applied pressure. Our results suggest that the intermittent formation of covalent bonds must be considered as an additional mechanism limiting the extraordinary lubrication by graphene at high contact pressure. On the other hand, the reversible switching between superlow and high-friction regimes opens opportunities to design micromechanical applications which require both low-friction sliding in contact and a wearless slowdown functionality.

Acknowledgments. Computing time was granted by the John von Neumann Institute for Computing (NIC) and provided on the supercomputer JUWELS at Jülich Supercomputing Centre (JSC) within the Project No. HFR09. Further computing time was provided by the State of Baden-Württemberg through bwHPC and the DFG (Grant No. INST 39/963-1 FUGG, bwForCluster NEMO). We acknowledge financial support by Deutsche Forschungsgemeinschaft within the Priority Program SPP 2244 “2DMP” (B.S. and R.B.) and within the Research Unit 5099 (M.M.); T.K. acknowledges the final supports from the JSPS Leading Initiative for Excellent Young Researchers and JST, PRESTO Grant No. JPMJPR22A6, Japan. Sample preparation by Thomas Seyller (University of Technology Chemnitz) is gratefully acknowledged.

-
- [1] D. Berman, A. Erdemir, and A. V. Sumant, Graphene: A new emerging lubricant, *Mater. Today* **17**, 31 (2014).
- [2] H. Kinoshita, Y. Nishina, A. A. Alias, and M. Fujii, Tribological properties of monolayer graphene oxide sheets as water-based lubricant additives, *Carbon* **66**, 720 (2014).
- [3] H. P. Mungse and O. P. Khatri, Chemically functionalized reduced graphene oxide as a novel material for reduction of friction and wear, *J. Phys. Chem. C* **118**, 14394 (2014).
- [4] K.-S. Kim, H.-J. Lee, C. Lee, S.-K. Lee, H. Jang, J.-H. Ahn, J.-H. Kim, and H.-J. Lee, Chemical vapor deposition-grown graphene: The thinnest solid lubricant, *ACS Nano* **5**, 5107 (2011).
- [5] D. Berman, S. A. Deshmukh, S. Sankaranarayanan, A. Erdemir, and A. V. Sumant, Macroscale superlubricity enabled by graphene nanoscroll formation, *Science* **348**, 1118 (2015).
- [6] Z. Liu, J. Yang, F. Grey, J. Z. Liu, Y. Liu, Y. Wang, Y. Yang, Y. Cheng, and Q. Zheng, Observation of Microscale Superlubricity in Graphite, *Phys. Rev. Lett.* **108**, 205503 (2012).
- [7] T. Filleter, J. L. McChesney, A. Bostwick, E. Rotenberg, K. V. Emtsev, K. Horn Th, and R. Bennewitz, Friction and Dissipation in Epitaxial Graphene Films, *Phys. Rev. Lett.* **102**, 086102 (2009).
- [8] C. Lee, Q. Li, W. Kalb, X.-Z. Liu, H. Berger, R. Carpick, and J. Hone, Frictional characteristics of atomically thin sheets, *Science* **328**, 76 (2010).
- [9] S. Li, Q. Li, R. W. Carpick, P. Gumbsch, X. Z. Liu, X. Ding, J. Sun, and J. Li, The evolving quality of frictional contact with graphene, *Nature (London)* **539**, 541 (2016).
- [10] Z. Ye, A. Balkanci, A. Martini, and M. Z. Baykara, Effect of roughness on the layer-dependent friction of few-layer graphene, *Phys. Rev. B* **96**, 115401 (2017).
- [11] A. Klemenz, L. Pastewka, S. G. Balakrishna, A. Caron, R. Bennewitz, and M. Moseler, Atomic scale mechanisms of friction reduction and wear protection by graphene, *Nano Lett.* **14**, 7145 (2014).
- [12] J. H. Ko, S. Kwon, I. S. Byun, J. S. Choi, B. H. Park, Y. H. Kim, and J. Y. Park, Nanotribological properties of fluorinated, hydrogenated, and oxidized graphenes, *Tribol. Lett.* **50**, 137 (2013).
- [13] Q. Y. Li, X. Z. Liu, S. P. Kim, V. B. Shenoy, P. E. Sheehan, J. T. Robinson, and R. W. Carpick, Fluorination of graphene enhances friction due to increased corrugation, *Nano Lett.* **14**, 5212 (2014).
- [14] K. V. Emtsev, A. Bostwick, K. Horn, J. Jobst, G. L. Kellogg, L. Ley, J. L. McChesney, T. Ohta, S. A. Reshanov, J. Rohrl, E. Rotenberg, A. K. Schmid, D. Waldmann, H. B. Weber, and T. Seyller, Towards wafer-size graphene layers by atmospheric pressure graphitization of silicon carbide, *Nat. Mater* **8**, 203 (2009).
- [15] T. Filleter, K. V. Emtsev, T. Seyller, and R. Bennewitz, Local work function measurements of epitaxial graphene, *Appl. Phys. Lett.* **93**, 133117 (2008).
- [16] E. Meyer, R. Bennewitz, and H. J. Hug, *Scanning Probe Microscopy: The Lab on a Tip*, Graduate Texts in Physics (Springer, Cham, 2021).
- [17] R. J. Cannara, M. J. Brukman, and R. W. Carpick, Cantilever tilt compensation for variable-load atomic force microscopy, *Rev. Sci. Instrum.* **76**, 053706 (2005).
- [18] T. Filleter and R. Bennewitz, Structural and frictional properties of graphene films on SiC(0001) studied by atomic force microscopy, *Phys. Rev. B* **81**, 155412 (2010).
- [19] See Supplemental Material at <http://link.aps.org/supplemental/10.1103/PhysRevResearch.5.L012049> for additional experiment and simulation results, additional data analyses, and a quantitative model to compare simulated shear stress and measured friction force.
- [20] M. Elstner, D. Porezag, G. Jungnickel, J. Elsner, M. Haugk, T. Frauenheim, S. Suhai, and G. Seifert, Self-consistent-charge density-functional tight-binding method for simulations of complex materials properties, *Phys. Rev. B* **58**, 7260 (1998).
- [21] Atomistica Software Suite, <http://www.atomistica.org>.
- [22] L. Pastewka, S. Moser, and M. Moseler, Atomistic insights into the running-in, lubrication, and failure of hydrogenated diamond-like carbon coatings, *Tribol. Lett.* **39**, 49 (2010).
- [23] D. Frenkel and B. Smit, *Understanding Molecular Simulation*, 2nd ed. (Academic Press, San Diego, 2002).
- [24] Y. Gao, T. F. Cao, F. Cellini, C. Berger, W. A. de Heer, E. Tosatti, E. Riedo, and A. Bongiorno, Ultrahard carbon film from epitaxial two-layer graphene, *Nat. Nanotechnol.* **13**, 133 (2018).
- [25] B. Luan and M. Robbins, The breakdown of continuum models for mechanical contacts, *Nature (London)* **435**, 929 (2005).

- [26] G. Brambilla and D. N. Payne, The ultimate strength of glass silica nanowires, *Nano Lett.* **9**, 831 (2009).
- [27] C. R. Kurkjian, P. K. Gupta, and R. K. Brow, The strength of silicate glasses: What do we know, what do we need to know?, *Int. J. Appl. Glass Sci.* **1**, 27 (2010).
- [28] A. P. M. Barboza, M. H. D. Guimaraes, D. V. P. Massote, L. C. Campos, N. M. B. Neto, L. G. Cancado, R. G. Lacerda, H. Chacham, M. S. C. Mazzoni, and B. R. A. Neves, Room-temperature compression-induced diamondization of few-layer graphene, *Adv. Mater.* **23**, 3014 (2011).
- [29] T. Hofmann, X. Ren, A. J. Weymouth, D. Meuer, A. Liebig, A. Donarini, and F. J. Giessibl, Evidence for temporary and local transition of sp^2 graphite-type to sp^3 diamond-type bonding induced by the tip of an atomic force microscope, *New J. Phys.* **24**, 083018 (2022).
- [30] Q. Li, Y. Dong, D. Perez, A. Martini, and R. Carpick, Speed Dependence of Atomic Stick-Slip Friction in Optimally Matched Experiments and Molecular Dynamics Simulations, *Phys. Rev. Lett.* **106**, 126101 (2011).
- [31] D. R. Tadjiev and R. J. Hand, Surface hydration and nanoindentation of silicate glasses, *J. Non-Cryst. Solids* **356**, 102 (2010).
- [32] D. Andersson and A. S. de Wijn, Understanding the friction of atomically thin layered materials, *Nat. Commun.* **11**, 420 (2020).
- [33] Y. Huang, Q. Yao, Y. Qi, Y. Cheng, H. Wang, Q. Li, and Y. Meng, Wear evolution of monolayer graphene at the macroscale, *Carbon* **115**, 600 (2017).
- [34] D. Marchetto, C. Held, F. Hausen, F. Wahlisch, M. Dienwiebel, and R. Bennewitz, Friction and wear on single-layer epitaxial graphene in multi-asperity contacts, *Tribol. Lett.* **48**, 77 (2012).